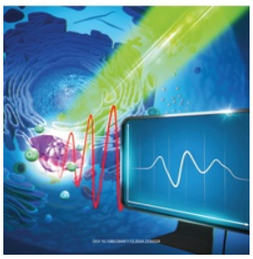
FUNCTIONAL DIAMOND



Functional Diamond

ISSN: 2694-1112 (Print) 2694-1120 (Online) Journal homepage: www.tandfonline.com/journals/tfdi20

Mosaic growth and characteristics of 2-inch single-crystal diamond

Caoyuan Mu, Xianyi Lv, Qiliang Wang, Xue Liu, Hua Fan, Jingyu Chen, Liuan Li, Bo Zou & Guangtian Zou

To cite this article: Caoyuan Mu, Xianyi Lv, Qiliang Wang, Xue Liu, Hua Fan, Jingyu Chen, Liuan Li, Bo Zou & Guangtian Zou (2026) Mosaic growth and characteristics of 2-inch single-crystal diamond, Functional Diamond, 6:1, 2620820, DOI: 10.1080/26941112.2026.2620820

To link to this article: https://doi.org/10.1080/26941112.2026.2620820

© 2026 The Author(s). Published by Informa UK Limited, trading as Taylor & Francis Group, on behalf of Zhengzhou Research Institute for Abrasives & Grinding Co., Ltd.

Published online: 25 Jan 2026.

Submit your article to this journal

Article views: 2124

View related articles

View Crossmark data

Citing articles: 1 View citing articles

Full Terms & Conditions of access and use can be found at
https://www.tandfonline.com/action/journalInformation?journalCode=tfdi20

FUNCTIONAL DIAMOND
2026, VOL. 6, NO. 1, 2620820
https://doi.org/10.1080/26941112.2026.2620820

Taylor & Francis
Taylor & Francis Group

RESEARCH ARTICLE

OPEN ACCESS Check for updates

Mosaic growth and characteristics of 2-inch single-crystal diamond

Caoyuan Mu[a], Xianyi Lv[a], Qiliang Wang[a], Xue Liu[a], Hua Fan[b], Jingyu Chen[b], Liuan Li[a], Bo Zou[a], and Guangtian Zou[a]

[a]State Key Laboratory of High Pressure and Superhard Materials, College of Physics, Jilin University, Changchun, China; [b]ZW Precision Mircofabrication Instruments (Shenzhen) Co. Ltd, Shenzhen, China

ABSTRACT

In this study, 2-inch single-crystal diamond (SCD) was fabricated *via* mosaic growth and laser stealth dicing. First, the growth behavior of 2 inch-scale diamond in an enclosed substrate holder was simulated, obtaining the spatial conditions conducive to continuous growth of large-area SCD. Subsequently, SCD wafers with dimensions of $50\times25\,mm^2$ and $48\times48\,mm^2$ were assembled through mosaic growth. Finally, the $48\times48\,mm^2$ SCD wafer was successfully and rapidly (approximately 40 min) detached by laser stealth dicing technology with a subsurface damage layer thickness of less than 100 micrometers.

Abbreviations: SCD: single-crystal diamond; MPCVD: microwave plasma chemical vapour deposition; OM: optical microscope; AFM: atomic force microscopy; FTIR: Fourier transform infrared spectroscopy; RC: rocking curve; RC: rocking curve; FWHM: full width at half maximum; PL: Photoluminescence

ARTICLE HISTORY
Received 1 December 2025
Accepted 19 January 2026

KEYWORDS
Mosaic growth; 2 inch; laser stealth dicing; single-crystal diamond

1. Introduction

The semiconductor serves as the foundation of modern industry, which providing crucial strategic support for the development of next-generation information technology, high-end equipment manufacturing, low-carbon technologies, the digital economy, and new materials [1]. Currently, as the Moore's law of silicon device approaches its limit, the semiconductor industry is experiencing unprecedented diversity in development. Diamond material is regarded as the ultimate semiconductor, featuring a high critical electric field (>10 MV/cm, 30 times that of silicon) and high carrier mobility (~3000 $cm^2{\cdot}V^{-1}{\cdot}s^{-1}$, twice that of silicon), enabling lower capacitance and on-state resistance at the same voltage level [2,3]. Additionally, diamond's thermal conductivity (~2200 $W{\cdot}m^{-1}{\cdot}K^{-1}$) far surpasses that of silicon, gallium nitride, silicon carbide, and gallium oxide, fundamentally addressing the heat dissipation challenges of devices. Consequently, diamond can be used to manufacture power electronic devices, high-power semiconductor lasers, integrated circuit components, solid-state microwave devices, and serve as heat-dissipating substrates for other semiconductor devices, enhancing the operating power and stability of power devices [4–6].

A key technical challenge limiting the industrialization of diamond materials and devices is the epitaxial growth of large area, high-quality SCDs. First, increasing wafer size theoretically reduces material loss during production processes, thereby improving utilization efficiency. Additionally, larger wafers enhance production efficiency, reduce costs, and improve yield rates. However, natural diamonds or those grown under high temperature and high pressure typically have sizes smaller than $15\times15\,mm^2$. Given diamond's exceptional potential in power device applications, large-scale diamond has become a focal point of global competition. In 2014, a Japan team expanded diamond dimensions to $40\times60\,mm^2$ using a "cloning" mosaic growth, though significant defects remained at the boundaries [7]. In 2017, a Germany team heteroepitaxy grew a 92 mm-diameter SCD on Ir/YSZ/Si [8]. In 2021, Kim et al. successfully obtained 2-inch SCD using a sapphire substrate [9]. In 2023, the research teams from China reported the growth of 2-inch SCDs on both silicon and sapphire substrates [10]. The advantage of heteroepitaxial growth is its ease in achieving large-scale diamond growth without the need for detachment, yet the significant differences in thermal expansion coefficients and lattice constants between the substrate and diamond can easily lead to higher internal stress and dislocation density [11,12]. While for the mosaic growth, although can achieve lower dislocation density due to the homoepitaxial approach, it faces challenges in further diameter

CONTACT Xianyi Lv lvxy@jlu.edu.cn; Qiliang Wang wangqiliang@jlu.edu.cn; Liuan Li liliuan@jlu.edu.cn; Bo Zou zoubo@jlu.edu.cn; Guangtian Zou gtzou@jlu.edu.cn State Key Laboratory of High Pressure and Superhard Materials, College of Physics, Jilin University, Changchun130012, China

© 2026 The Author(s). Published by Informa UK Limited, trading as Taylor & Francis Group, on behalf of Zhengzhou Research Institute for Abrasives & Grinding Co., Ltd.
This is an Open Access article distributed under the terms of the Creative Commons Attribution-NonCommercial License (http://creativecommons.org/licenses/by-nc/4.0/), which permits unrestricted non-commercial use, distribution, and reproduction in any medium, provided the original work is properly cited. The terms on which this article has been published allow the posting of the Accepted Manuscript in a repository by the author(s) or with their consent.

expansion due to issues such as defects and stress near the boundaries and the following detach processes. The "cloning" mosaic growth method utilizes cutting or ion implantation techniques to obtain seeds with nearly identical crystallographic properties from the same SCD, effectively suppressing stress and defects at the boundaries during growth [13]. However, "cloning" requires high-energy ion implantation assistance for seed detachment, which can introduce new defects and involves complex processes. Additionally, traditional laser cutting methods are unable to achieve low-damage detachment of 2-inch diamond crystals.

In our previous work, we investigated the influence of step flow direction on the mosaic growth and found that boundaries near seeds with significant differences in step flow orientation exhibit competitive growth, while boundaries formed by seeds with similar orientations coalescence well through step flow growth [14]. Furthermore, by using this step flow modulation technology, we can simplify the seed crystal selection process and initially achieve the mosaic growth of 1-inch SCD. On this basis, we simulated the growth behavior of inch-scale diamond in an enclosed substrate holder using COMOSOL software, obtaining the spatial position suitable for continuous growth of large area SCD. Subsequently, single-crystal diamond (SCD) wafers with dimensions of $50 \times 25\,mm^2$ and $48 \times 48\,mm^2$ were fabricated *via* mosaic growth. Finally, the $48 \times 48\,mm^2$ SCD wafer was successfully and rapidly detached by laser stealth dicing technology with a subsurface damage layer thickness of less than 100 μm.

2. Experimental detail

The experiment was conducted in a commercial 2.45 GHz 10 kW microwave plasma chemical vapour deposition (MPCVD) system (as shown in Figure 1). Microwaves are fed in through a coaxial antenna, and a circular quartz glass is located below the water-cooled copper stage away from the etching of the plasma. The inlet and outlet are located at the top and the bottom of the cavity, respectively. Observation windows are arranged on both sides, and the plasma converges directly above the molybdenum substrate holder. The operation modes and electromagnetic field distribution within the MPCVD cavity were simulated by adopting the COMSOL Multiphysics 6.2 software platform as reported in our previous work [15]. In the two-dimension axisymmetric simulations, a coaxial port was used as the microwave excitation with perfect electric conductors as cavity boundaries. At an operation power of 10 kW, the plasma in the butterfly cavity is uniformly distributed above the substrate holder, with a relatively weak secondary electric field (Figure 1(a)). A comparison with the electric field distribution diagram of the intrinsic modes in the cylindrical cavity reveals that our device's electric field distribution is dominated by the TM_{022} mode (Figure 1(b)).

The precursor gases are a mixture of H_2, CH_4, N_2, O_2, and Ar. The purity is 99.99999% after purification for the H_2 and CH_4, N_2 is a 1% dilution gas diluted with H_2, and the purity of O_2 and Ar is 99.999%. The flow rates of mixed gases are set to 400:20:0.02:1.3:10 sccm. The power, chamber pressure, and growth temperature are 8 kW, 140 Torr, and 1100 °C, respectively. The substrates are home-made 1-inch ($25 \times 25 \times 0.5\,mm^3$) SCD. Before growth, the substrate was ultrasonically cleaned in acetone and ethanol for 30 min to remove organic pollutants. After drying with nitrogen, each sample is fixed on an enclosed substrate holder and then loaded into a chamber with a background vacuum of 10^{-4} Torr. Before the growth of diamond films, the substrate is etched in H_2 plasma at 1000 °C for 20 min to remove surface contaminants and polish damage. The conventional laser cutting is used to detach the epitaxial layer on the 1-inch SCD. The specific parameters are laser wavelength, power, and frequency of 532 nm, 12 W, and 10 kHz, respectively. By combining step flow modulation technology, 1-inch diamond can be enlarged into $50 \times 25\,mm^2$ and $48 \times 48\,mm^2$ SCD wafers *via* mosaic growth. To calculated the dislocation density, the SCD were subjected to H_2-O_2 plasma etching under conditions of H_2:O_2 of 400:8 sccm, temperature of 900 °C, and duration of 30 min. The laser stealth dicing was adopted to detach

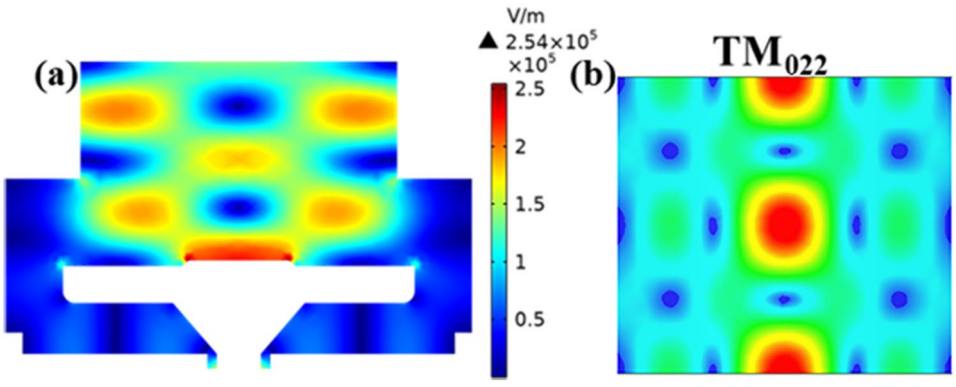


Figure 1. (a) The plasma distribution in the cavity at an operation power of 10 kW. (b) The electric field distribution diagram of the intrinsic TM_{022} mode in the cylindrical cavity.

the $48 \times 48 \times 0.35\ mm^3$ SCD after growth and polishing. The stealth dicing technology combines the advantages of multi-pulse laser system and optical shaping system, which can accurately focus the laser inside the diamond to form micro-stress modified layer. By precisely controlling the direction and intensity of stress, low loss slicing of large area diamonds can be achieved. The specific parameters are laser wavelength, power, and frequency of 1030 nm, 1.2 W, and 200 kHz, respectively.

We observe the surface morphology of the sample through an optical microscope (OM) and atomic force microscopy (AFM, Bruker Dimension ICON). The transmittance of the sample was measured by Fourier transform infrared spectroscopy (FTIR) with a spectral resolution of $4\ cm^{-1}$. The X-ray rocking curve (RC) and the derived full width at half maximum (FWHM) are used to evaluate the crystalline quality and the step of mapping test is approximately 3 mm. Photoluminescence (PL) and Raman spectroscopy (HORIBA HRS-750) were collected using a 532 nm laser and a 500/1200 groove/mm grating. Mapping measurements were performed using a Raman microscope (Renishaw inVia) with a laser wavelength of 532 nm, an 1800 g/mm grating, and a testing step of approximately 1 mm.

3. Results and discussions

During the high-speed and high-quality epitaxial growth of SCD, the plasma aggregation phenomenon at the edge of the seed leads to polycrystalline rims. It is usually necessary to adopt an enclosed substrate holder to weaken the attraction of the seed edge to the plasma. Previously, we found that the spatial position of the seed in the substrate holder significantly affects its growth mode of the $7 \times 7\ mm^2$ SCD, and there is a "single-crystal growth zone" when optimizing the width and depth parameters [16]. Therefore, we used the COMOSOL software to investigate the effect of the spatial position of 2 inch-sized SCD on plasma distribution in an enclosed substrate holder, and confirmed the appropriate range for continuous growth of SCD. First, a certain seed depth was maintained (the diamond surface was 0.5 mm below the substrate holder surface), and the effect of the width between the seed and the holder on the plasma distribution was investigated (Figure 2). When the width increases to a certain value (2.5 mm for an example), the plasma cannot be effectively transferred by the substrate holder and aggregates at the edge of the diamond to form a polycrystalline rim (Figure 2(a,d)). When the width is appropriately decreased (1.5 mm for an example), the plasma is simultaneously attracted by the diamond edge and the substrate holder, and the plasma distribution on the diamond seed surface is uniform, achieving good growth conditions and maintaining SCD status (Figure 2(b,d)). When the width is relatively small, the substrate holder and the diamond edge is very close and the plasma tends to concentrate more at the edge of the substrate holder. The decrease in plasma density and the heat dissipation effect of the substrate holder result in a low temperature and low concentration of growth radicals, ultimately suppressing the growth of seed edges (Figure 2(c,d)).

Furthermore, we maintained a certain width (with a spacing of 1.5 mm between the seed and the substrate holder) and investigated the effect of the depth of the seed on the plasma distribution (Figure 3). When the depth of the seed is relatively small, the attracting and dispersing plasma of the substrate holder decreases, and high-density plasma accumulates at the edge of the diamond, which significantly increases the growth temperature in this area and forms polycrystalline rim (Figure 3(a,d)). The diamond edge is away from the plasma discharge area when the depth of the seed increases to an appropriate range, which is conducive to the transfer of plasma to the substrate holder (Figure 3(b,d)). Thus, it is possible to achieve uniform distribution of plasma at the edges and surfaces of diamond. As the depth further increases, the plasma undergoes excessive transfer to the substrate holder, resulting in a decrease in plasma density at the diamond edge (Figure 3(c,d)). At the same time, the substrate holder can assist in heat dissipation, leading to a decrease in growth rate at the edge. In summary, there is a relatively optimal range for the depth and width of the seed in the enclosed substrate

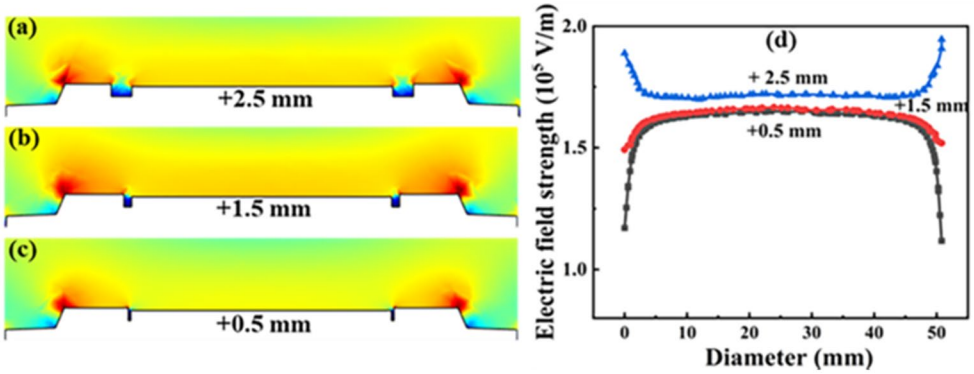


Figure 2. (a–c) The plasma distribution in the cavity with widths of 2.5, 1.5, and 0.5 mm between the seed and the holder, respectively. (d) The electric field profiles along the diamond surface with different widths.

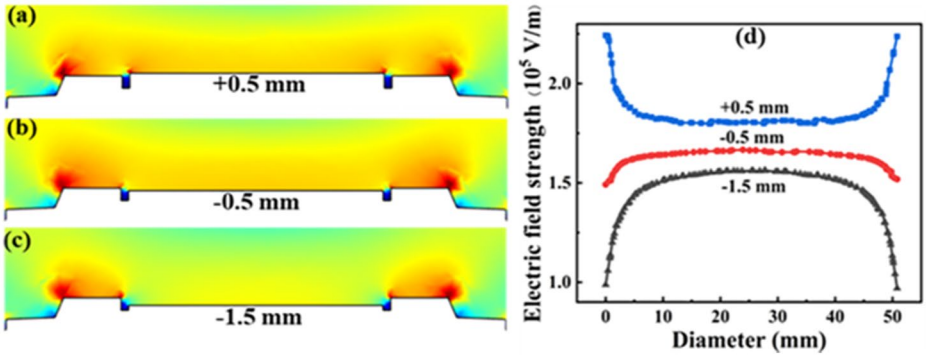


Figure 3. (a–c) The plasma distribution in the cavity with depths of +0.5, −0.5, and −1.5 mm between the seed and the holder, respectively. (d) The electric field profiles along the diamond surface with different depths.

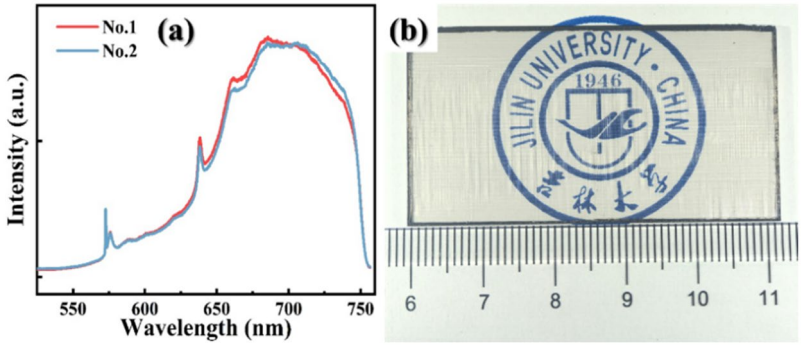


Figure 4. (a) The PL spectra of the two 1-inch SCD seeds after laser cutting and polishing. (b) The optical photo of the 50 × 25 mm^2 SCD obtained by mosaic growth.

holder, which can ensure uniform distribution of surface plasma and effectively maintain the growth state of the single-crystal. This is consistent with our previous experimental conclusions.

Based on the optimized substrate holder structure and spatial position parameters of the seed, we continuously grew a 1-inch SCD for 60 h (growth rate of about 10 μm/h) in our experiment. The remaining thickness of the detached SCD seed is approximately 500 μm because of the laser cutting and polishing loss. The two seeds obtained by repeat growth exhibit similar PL spectra (Figure 4(a)), with a diamond first-order Raman peak at 572 nm, an NV^0 zero phonon line at 575 nm, and an NV^- zero phonon line at 638 nm, while the SiV^- zero phonon line at 738 nm is almost invisible [17,18]. The nitrogen-related PL peak originates from the addition of nitrogen gas during the growth process in order to increase the growth rate and maintain (100) faces [19]. Furthermore, we modulate the step flow direction of the two SCDs and complete the mosaic growth, as shown in Figure 4(b). The obtained 50 × 25 mm^2 SCD material exhibits good transparency, indicating that the relatively low nitrogen content did not result in significant color changes. At the same time, there are no visible defects on the surface and around the boundary, indicating that the boundary can achieve effective coalescence under this growth condition.

The crystalline quality and stress state of the 50 × 25 mm^2 SCD can be characterized by Raman mapping testing, with a testing range of 1 × 1 mm^2 and a step of 20 μm near the boundary (Figure 5). We can observe that the diamond Raman peak position (around 1332 cm^{-1}) of the epitaxial layer near the boundary shows good uniformity and is consistent with the epitaxial layer above substrate, which proves that there is no additional internal stress in the boundary (Figure 5(a)). The deduced FWHM mapping results indicate that the values near the boundary are about 2.4–2.5, which is only slightly higher than of the epitaxial layer above substrate (2.0–2.2) (Figure 5(b)). This proves that no obvious crystalline quality degradation occurs around the boundary because of the good coalescence of the epitaxial layer. The XRD rocking curve is also fitted with a FWHM of 0.0488° (Figure 5(c)). The dislocation density calculated by the density of etching pits is approximately 1.1 × 10^5 cm^{-2}. Meanwhile, the infrared transmittance test indicates that the overall transmittance is about 60%, except for the intrinsic absorption peaks of diamond near 2–4 μm (Figure 5(d)) [20]. After the mosaic growth, the sample detached by laser cutting but the cutting side is only cleaned with acid solution and plasma etching in CVD system to remove the carbon layer. Polishing of the cutting side was not carried out to avoid the cracking due to the relatively small thickness of the detached layer. In addition, during the epitaxial growth process, we added some nitrogen to promote the growth of (100) plane. Although no obvious nitrogen absorption peaks were observed at 1130 and 1344 cm^{-1} [21,22], the small amount of nitrogen during the mosaic growth also reduces the transmittance to a certain extent.

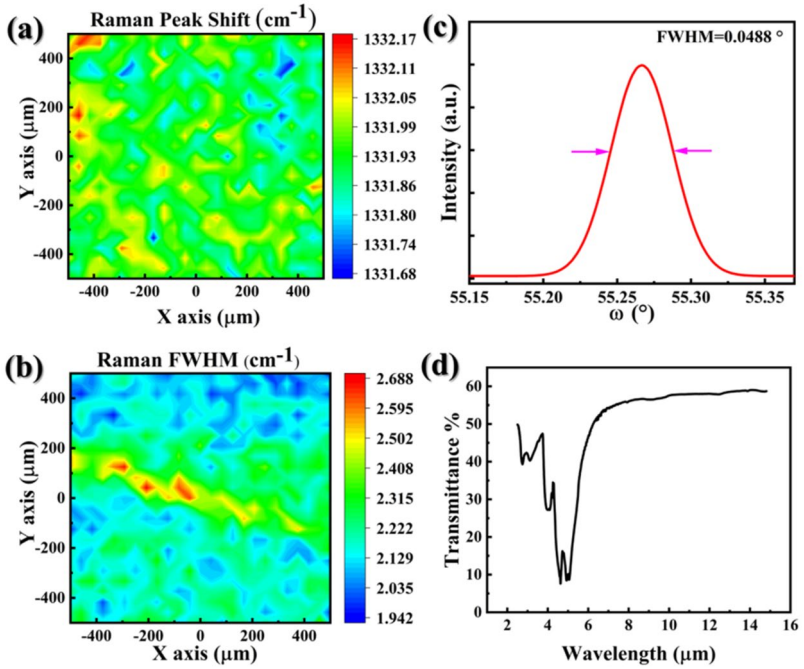


Figure 5. The Raman peak position mapping (a), Raman FWHM mapping (b), typical XRD rocking curve (c) and infrared transmittance test (d) of the $50 \times 25\,mm^2$ mosaic SCD.

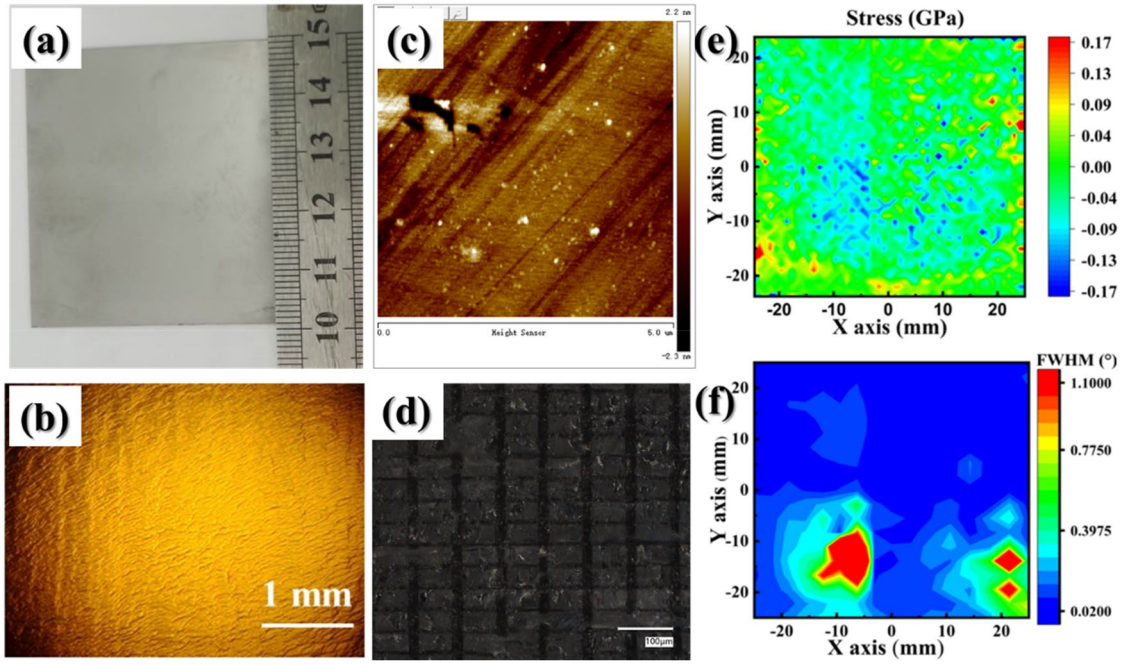


Figure 6. The optical photo (a) and surface morphology (b) of the $48 \times 48\,mm^2$ mosaic SCD before laser stealth dicing. (c) and (d) are the AFM on the polished surface and the optical photo of the backside. (e) and (f) are stress calculated from Raman peak position, and XRD rocking curve mapping.

Similar to the mosaic processing of 1-inch SCD, we can obtain two $50 \times 25\,mm^2$ SCDs by setting reasonable seed spatial parameters for epitaxial growth and then laser cutting, thereby achieving the mosaic growth of $48 \times 48\,mm^2$ SCD. The optical photograph of the $48 \times 48 \times 0.35\,mm^3$ SCD obtained by laser stealth dicing is shown in Figure 6. It can be seen that the SCD wafer has a flat surface with no obvious polycrystalline rim growth at the edges (Figure 6(a)). The successes coalescence of step flow at the boundaries indicates that the optimized conditions are also applicable to the growth of 2-inch SCDs. In order to characterize the stress state and crystalline quality of SCD in detail, the obtained diamond was subjected to Raman and rocking curve mapping tests (Figure 6(b)). The AFM measurement demonstrates that no obvious boundary is observed on the top surface excepting the polishing scratch, showing an average roughness of around 0.5 nm in the

$5 \times 5\,\mu m^2$ scale (Figure 6(c)). On the other hand, the backside after laser stealth dicing presents an average roughness of approximately 5 µm. In addition, the widths of the lateral and vertical cutting lines are approximately 8 and 18 µm, respectively (Figure 6(d)). It can be found that the Raman peak positions of the entire single-crystal material are relatively close distributed (around $1332.5\,cm^{-1}$), except for a few regions where there is a peak position shift phenomenon. The stress distribution (σ) of the SCD can be calculated according to the formula of $\sigma = -0.34 \times \Delta\nu$ (GPa) (where $\Delta\nu = \nu - 1332.5\,cm^{-1}$) [23]. As shown in Figure 6(e), most of the SCD presents only a small compress stress of approximately 0.04 GPa. In addition, the peak positions around the boundaries are almost identical to that of epitaxial layer above the substrate, indicating that the step flow modulation can achieve good coalescence and low internal stress. The rocking curve mapping results also show that the distribution of FWHM (approximately 0.03 degree) of the entire SCD is relatively close except for a few areas (Figure 6(f)), indicating that the obtained SCD exhibits good crystalline quality. The region with high FWHM value has the same position on the two 1-inch substrate surface, which is due to the non-epitaxy points in the region during epitaxial growth. The defect is not completely transformed into single crystal in the subsequent mosaic growth process.

4. Conclusions

The influence of the depth and width of seed in an enclosed substrate holder on plasma distribution and subsequent growth were simulated *via* COMOSL software. The results indicate that when the depth and width of the seed fall within an optimal range, plasma transfers from the seed crystal edges to the substrate holder, leading to a more uniform plasma distribution on the diamond surface and suppressing localized high-temperature region, ultimately yielding well-grown SCDs. However, when the depth exceeds a critical value or the width falls below a critical value, the plasma is excessively attracted by the substrate holder, resulting in reduced plasma concentration and temperature at the seed crystal edges, thereby limiting growth. Based on these findings, our achievements enabled long-term continuous growth and laser-cutting separation of 1-inch SCDs, while also providing high-quality seeds for further mosaic growth.

Subsequently, $50 \times 25\,mm^2$ and $48 \times 48\,mm^2$ SCDs were successfully fabricated using the mosaic growth method and their crystal quality was characterized. The Raman peak positions and FWHM distributions at the boundaries of the $50 \times 25\,mm^2$ SCD were relatively uniform and closely matched those of the epitaxial layer above seed. Using laser stealth dicing technology, the epitaxial layer of the $48 \times 48\,mm^2$ SCD was successfully separated from the substrate. The sample surface exhibited typical step-flow growth, low stress and high crystalline quality.

CrediT

Caoyuan Mu: Methodology, Formal analysis, Investigation, Writing–original draft. Xianyi Lv: Conceptualization, Writing–review & editing. Xue Liu: Methodology, Writing – review & editing. Qiliang Wang: Methodology. Hua Fan: Methodology. Jingyu Chen: Methodology. Liuan Li: Formal analysis, Writing–review & editing. Bo Zou: Funding acquisition & Resources. Guangtian Zou: Funding acquisition, Resources, Writing – review & editing.

Disclosure statement

The authors declare no conflict of interest.

Funding

This work was supported by the Research and Development Program of Hainan Province (No. ZDYF2025SXLH014) and the Fundamental and Interdisciplinary Disciplines Breakthrough Plan of the Ministry of Education of China.

Notes on contributors

Caoyuan Mu: Student of State Key Laboratory of High Pressure and Superhard Materials, College of Physics, Jilin University.

Xianyi Lv: Research fellow of State Key Laboratory of High Pressure and Superhard Materials, College of Physics, Jilin University.

Qiliang Wang: Research fellow of State Key Laboratory of High Pressure and Superhard Materials, College of Physics, Jilin University.

Xue Liu: Student of State Key Laboratory of High Pressure and Superhard Materials, College of Physics, Jilin University.

Hua Fan: Engineer of ZW Precision Mircofabrication Instruments (Shenzhen) Co. Ltd.

Jingyu Chen: Director of ZW Precision Mircofabrication Instruments (Shenzhen) Co. Ltd.

Liuan Li: Associate research fellow of State Key Laboratory of High Pressure and Superhard Materials, College of Physics, Jilin University.

Bo Zou: Professor of State Key Laboratory of High Pressure and Superhard Materials, College of Physics, Jilin University.

Guangtian Zou: Professor of State Key Laboratory of High Pressure and Superhard Materials, College of Physics, Jilin University.

ORCID

Liuan Li http://orcid.org/0000-0002-3407-6404

References

[1] Saito W. A future outlook of power devices from the viewpoint of power electronics trends. IEEE Trans

Electron Devices. 2024;71(3):1356–1364. doi: 10.1109/TED.2023.3332611
[2] Woo K, Bian Z, Noshin M, et al. From wide to ultrawide-bandgap semiconductors for high power and high frequency electronic devices. J Phys Mater. 2024;7(2):022003. doi: 10.1088/2515-7639/ad218b
[3] Isberg J, Hammersberg J, Johansson E, et al. High carrier mobility in single-crystal plasma-deposited diamond. Science (1979). 2002;297(5587):1670–1672. doi: 10.1126/science.1074374
[4] Li G, Lin W, Liu S, et al. Recent developments and challenges of edge termination techniques for vertical diamond schottky barrier diodes. Sensors. 2025;25(22):6974. doi: 10.3390/s25226974
[5] Dang C, Lu A, Wang H, et al. Diamond semiconductor and elastic strain engineering. J Semicond. 2022;43(2):021801. doi: 10.1088/1674-4926/43/2/021801
[6] Chang X, Gao W, An J, et al. Optical-grade diamond: characteristics, synthesis, and recent research progress. Funct Diamond. 2025;5(1):2476690. doi: 10.1080/26941112.2025.2476690
[7] Yamada H, Chayahara A, Mokuno Y, et al. A 2-in. mosaic wafer made of a single-crystal diamond. Appl Phys Lett. 2014;104(10):102110. doi: 10.1063/1.4868720
[8] Schreck M, Gsell S, Brescia R, et al. Ion bombardment induced buried lateral growth: the key mechanism for the synthesis of single crystal diamond wafers. Sci Rep. 2017;7(1):44462. doi: 10.1038/srep44462
[9] Kim S-W, Takaya R, Hirano S, et al. Two-inch high-quality (001) diamond heteroepitaxial growth on sapphire (1120) misoriented substrate by step-flow mode. Appl Phys Express. 2021;14(11):115501. doi: 10.35848/1882-0786/ac28e7
[10] Qu P, Jin P, Zhou G, et al. Growth of two-inch free-standing heteroepitaxial diamond on Ir/YSZ/Si (001) substrates via laser-patterned templates. J Semicond. 2024;45(9):090501. doi: 10.1088/1674-4926/24060003
[11] Dong C, Zhang K, He L, et al. Interfacial improvement of Ir/MgO substrate by post-deposition annealing for heteroepitaxial growth of single crystal diamond. J Alloys Compound. 2025;1036:182174. doi: 10.1016/j.jallcom.2025.182174
[12] Gallheber B-C, Klein O, Fischer M, et al. Propagation of threading dislocations in heteroepitaxial diamond films with (111) orientation and their role in the formation of intrinsic stress. J Appl Phys. 2017;121(22):225301. doi: 10.1063/1.4985174
[13] Yamada H, Chayahara A, Umezawa H, et al. Fabrication and fundamental characterizations of tiled clones of single-crystal diamond with 1-inch size. Diamond Relat Mater. 2012;24:29–33. doi: 10.1016/j.diamond.2011.09.007
[14] Li G, Li D, Mu C, et al. Effect of step-flow modulation on the large-size single crystal diamond through mosaic growth. Functional Diamond. 2023;3(1):2279057. doi: 10.1080/26941112.2023.2279057
[15] Liu X, Mu C, Wang Q, et al. Demonstration of a novel high-power MPCVD reactor using combined TM01 and TM02 modes for efficient diamond growth. Vacuum. 2025;242:114761. doi: 10.1016/j.vacuum.2025.114761
[16] Xie W, Lv X, Wang Q, et al. Relationship between the spatial position of the seed and growth mode for single-crystal diamond grown with an enclosed-type holder. Chinese Phys B. 2022;31(10):108106. doi: 10.1088/1674-1056/ac7e35
[17] Tallaire A, Collins A, Charles D, et al. Characterisation of high-quality thick single-crystal diamond grown by CVD with a low nitrogen addition. Diamond Relat Mater. 2006;15(10):1700–1707. doi: 10.1016/j.diamond.2006.02.005
[18] Mu C, Li G, Lv X, et al. Effect of hydrogen flow rate on the plasma state and quality of diamond crystals grown by MPCVD. Mater Sci Semicond Process. 2025;185:108884. doi: 10.1016/j.mssp.2024.108884
[19] De Theije F, Schermer J, Van Enckevort WJP. Effects of nitrogen impurities on the CVD growth of diamond: step bunching in theory and experiment. Diamond Relat Mater. 2000;9(8):1439–1449. doi: 10.1016/S0925-9635(00)00261-2
[20] Piccirillo C, Davies G, Mainwood A, et al. The variation of optical absorption of CVD diamond as a function of temperature. Physica B. 2001;308–310:581–584. doi: 10.1016/S0921-4526(01)00741-4
[21] Zaitsev A, Moe K, Wang W. Defect transformations in nitrogen-doped CVD diamond during irradiation and annealing. Diamond Relat Mater. 2018;88:237–255. doi: 10.1016/j.diamond.2018.07.017
[22] Johnson P, Moe KS, Persaud S, et al. Spectroscopic characterization of yellow gem quality CVD diamond. Diamond Relat Mater. 2023;140:110505. doi: 10.1016/j.diamond.2023.110505
[23] Li H, Zhang T, Li L, et al. Investigation on crystalline structure, boron distribution, and residual stresses in freestanding boron-doped CVD diamond films. J Cryst Growth. 2010;312(12–13):1986–1991. doi: 10.1016/j.jcrysgro.2010.03.020